Space-Energy Digital-Coding Metasurface Based on an Active Amplifier

Lei Chen,[1] Qian Ma,[2] Hong Bo Jing,[2] Hao Yang Cui,[1] Yi Liu,[3,*] and Tie Jun Cui[2,†]

[1]*College of Electronics and Information Engineering, Shanghai University of Electric Power, Shanghai 200090, China*

[2]*State Key Laboratory of Millimeter Wave, Southeast University, Nanjing 210096, China*

[3]*School of Information Science and Technology, Fudan University, Shanghai 200433, China*

(Received 9 February 2019; revised manuscript received 5 April 2019; published 20 May 2019)

The metasurface has aroused broad enthusiasm due to its splendid properties for electromagnetic (EM) wave manipulations. However, most previous metasurfaces, including passive and active metasurfaces, are almost energy losing when controlling EM waves. Some amplifying metasurfaces have been proposed, but the amplification function is uncontrollable. Here, we propose a spatial-energy digital-coding metasurface with active amplifiers to realize arbitrary editing of the energy of spatial propagating waves. Based on the proposed metasurface, the spatial energy of a linearly polarized propagating wave can not only be amplified, but can also be edited into arbitrary magnitudes (including amplification and reduction) by controlling the voltage. A metasurface element integrated with an amplifier chip is designed for energy modulations in the microwave frequency range. The numerical simulations and experimental results show good consistency, validating the feasibility of our design.

DOI: 10.1103/PhysRevApplied.11.054051

I. INTRODUCTION

Metasurfaces are artificially planar structures consisting of subwavelength elements, which provide amplitude and phase variations of transmitted, reflected, and scattered waves on the metasurface interface [1–3]. By controlling the amplitude and phase responses of each element, metasurfaces have the capacity to manipulate electromagnetic (EM) waves effectively in various ways and realize novel applications such as flat lens [4–6], perfect absorbers [7], imaging [8,9], and detection [10]. In particular, the generalized Snell's law [11], reveals the reflection and refraction mechanism of interaction between light and metasurfaces. Recently, the concept of a digital-coding metasurface [12] was proposed, which introduces a digital characterization to the metasurface and describes the unit cell by the digital coding "0" and "1," indicating opposite phase responses. Based on this concept, some remarkable studies have been presented, such as digital signal processing [13] and information theory [14] in metasurface designs. Moreover, the digital-coding metasurface provides a simpler way to steer EM waves and achieve a series of functions such as communication [15], imaging [16], anomalous reflections [17,18], and vortex-beam generation [19].

As a crucial means to manipulate the EM wave, amplitude-modulation metasurfaces have been verified that have the capability of controlling the intensity of the diffraction order [20], modifying acoustic radiation patterns [21], and enabling optical holography [22,23]. For passive metasurfaces, the most general strategy to modulate the amplitude is by changing the electrical mechanism, from which various methods for manipulating metasurfaces such as transparent conducting oxide, graphene and liquid crystal have been proposed to achieve dynamic beam-steering [24], a perfect absorber [25], and a multifunctional photonic switch [26]. However, such passive metasurfaces can only perform subtraction operations on the energy of the spatial EM wave, which limits their application potential. In addition to the above-mentioned amplitude-control methods, some metasurfaces based on active devices have also been realized. Researchers have recently introduced an amplifying circuit into metasurfaces to realize nonmagnetic nonreciprocal metasurfaces [27,28]. However, these works mainly focus on the nonreciprocity and neglect the modulation properties of the active amplifiers. Some amplifying metasurfaces based on a gain medium have been proposed [29,30] to realize power amplification.

The conventional manipulation on the energy of EM waves mainly focuses on the decrement in modulation such as in absorbers, but there is a lack of increments in modulations. The only way to enhance the energy is by increasing the source power, which is limited and demands an extra workload for the source feed. In fact, the modulation capacity of a power amplifier (PA) can greatly strengthen the tunability of a metasurface, which can easily be used in imaging or communication applications

*ylius@fudan.edu.cn

†tjcui@seu.edu.cn

based on metasurfaces. In this paper, we present a coding metasurface integrated with a PA to control the amplitude of EM waves more flexibly. By controlling the supply voltage of the PA, the amplitude of the spatial waves can be tailored either by increasing or decreasing the power level. Based on the board-level circuit components and printed-circuit-board (PCB) fabrication, the presented metasurface yields lower cost and easier fabrication. The measured results have good agreement with our analyses, which validates our design. This work may pave the way for energy modulation using digital-coding metasurfaces and may have potential in microwave imaging, detection, and other applications.

II. PRINCIPLE AND DESIGN

Figure 1 shows a schematic diagram of the presented digital-coding metasurface, integrated with chip amplifiers. When the whole system is excited by linearly polarized incidence from a feed horn, the spatial EM wave captured by the metasurface passes through the embedded amplifier, whose amplification level can be controlled by the supply voltage. As a result, the transmitting wave can be edited as desired, either in increment or decrement mode. Moreover, by applying specific controlling voltages, the spatial energy of the transmitted beam can be modulated into the required values, and these specific magnitudes can be further encoded into digits such as "00," "01," "10," and "11," which represent a certain amount of information.

To realize the aforementioned idea, we design a coding meta-atom at 5 GHz integrated with two chip amplifiers (Qorvo TQP369180), as shown in Fig. 2. The detailed structure of the presented element is provided in Fig. 2(a), in which the dimensions of a, h, and R are 40, 1, and

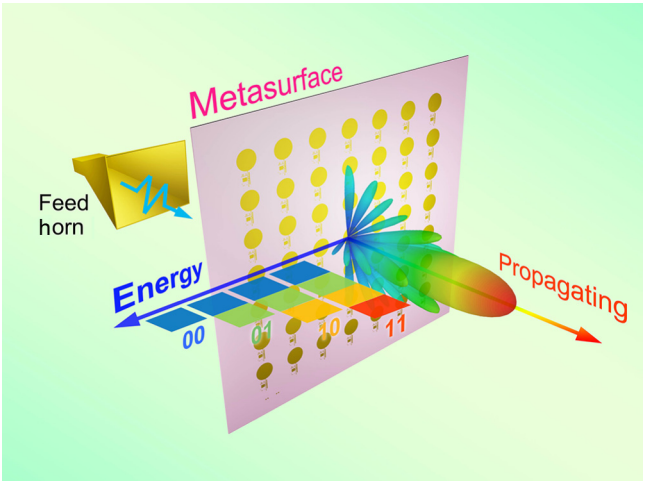

FIG. 1. A schematic diagram of the presented digital-coding metasurface. The magnitude of the transmitted wave can be manipulated by the metasurface integrated with chip amplifiers.

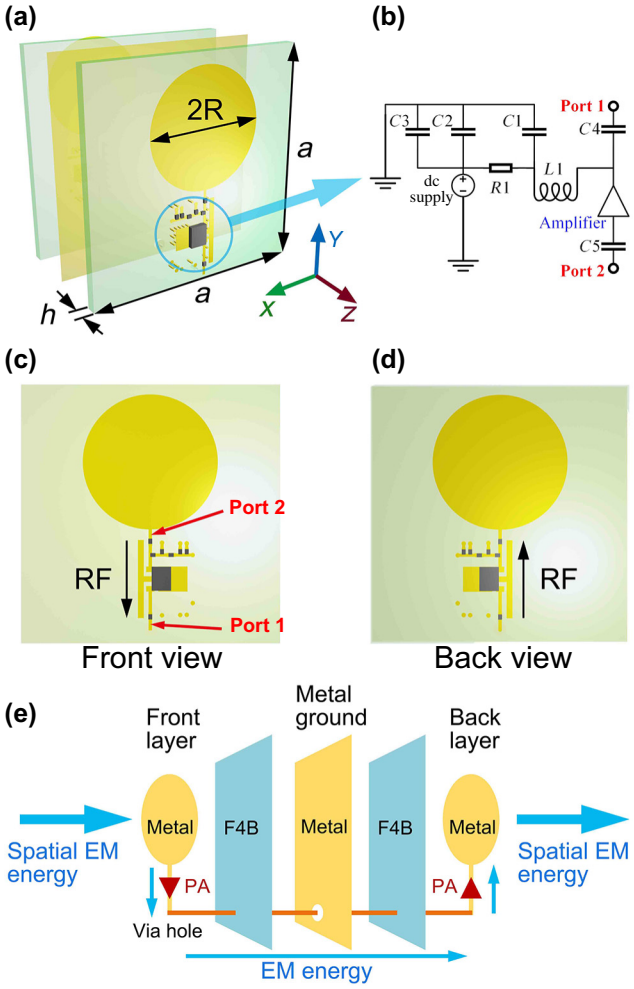

FIG. 2. The designed structure of the digital-coding element. (a) The detailed structure of the element. (b) A schematic diagram of the amplifier and its peripheral circuit. (c),(d) The front and back views of the designed element. (e) A detailed illustration of the element structure and energy transmission.

10.38 mm, respectively. The element is a sandwichlike structure, composed of Polytetrafluoroethylene (F4B, with a dielectric constant of 2.65 and loss tangent of 0.001), metal ground, and F4B. Please note that the polarization of the incident wave is along the y axis. Two amplifiers are embedded on the front and back layers of the meta-atom, and the related peripheral circuit is provided in Fig. 2(b). The values of $C1$, $C2$, $C3$, $C4$, $C5$, $L1$, and $R1$ are 18 nF, 1 nF, 1 μF, 56 pF, 56 pF, 39 nH and 24 Ω, respectively. The front and back views are given in Figs. 2(c) and 2(d), which indicate the transmitting direction of the radiofrequency (rf) signal. To clearly exhibit the energy-transmitting process, we provide a detailed structure of the element and its energy-transmitting route in Fig. 2(e). The spatial EM wave energy is captured by the front metal patch and is amplified by the first amplifier. Then the EM energy transmits through the via hole to the back layer and is amplified

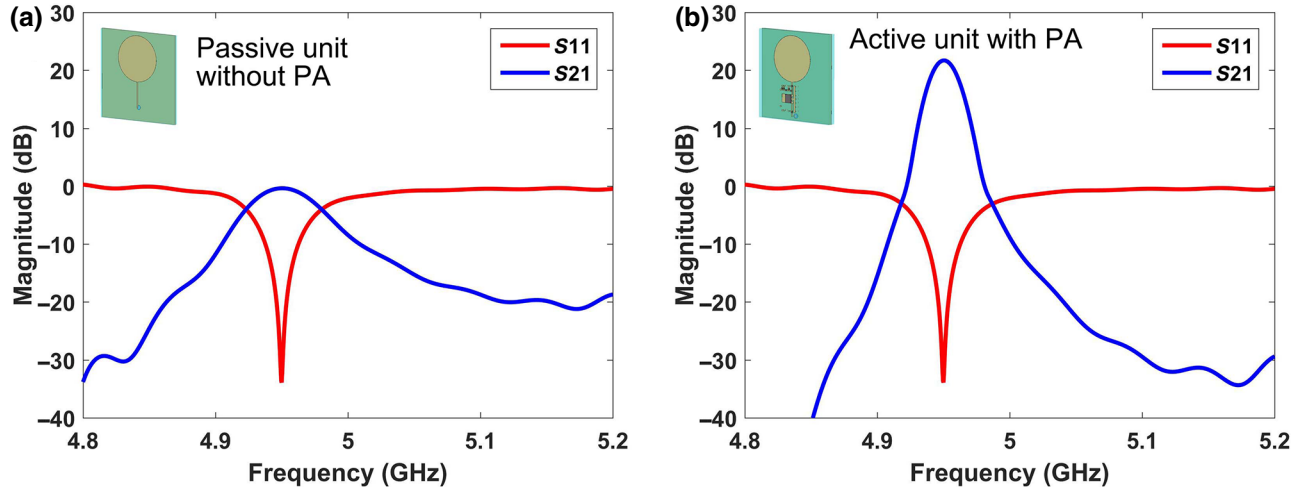

FIG. 3. The simulated S parameters of the designed coding element. (a) The passive structure of the coding element, without the amplifier. (b) The active element with the amplifier.

by the second amplifier. Finally, the energy is radiated back into space.

III. SIMULATIONS AND EXPERIMENTS

To demonstrate our design, we perform numerical simulations in commercial software, CST MICROWAVE STUDIO. For element simulation, the EM-circuit co-simulation in CST is applied to combine the EM components and active amplifier. The scattering parameter of the PA is firstly measured within the transmission reflection line measurement, and then it is embedded into the two-port component for the simulation. The element simulation applies the periodic boundary condition and plane-wave excitation. The operating frequency is set at 5 GHz. Figure 3 provides the simulated S parameters for the designed structure without and with PA, to demonstrate its amplification performance. The $S11$ and $S21$ results of the passive structure are illustrated in Fig. 3(a), suggesting that the resonant frequency is 4.95 GHz. At this frequency, this structure has greatest transmitting efficiency. When the PA chip is embedded into the element structure, the transmitting power is dramatically amplified by more than 20 dB, verifying the validity of the proposed element.

In our work, we mainly focus on the controllable amplification of PA, by applying different supply voltages. To further illustrate the manipulation performance of the element with the controllable PA, we provide the electric field results in the near- and far-field regions (eight wavelengths from front to back) for the designed element. To clearly exhibit the performance of amplitude modulation, four different amplification levels are selected as -10, 0, 10, and 20 dB, as shown in Figs. 4(a)–4(d), respectively. The reason we set a difference factor of 10 dB is to show the good performance and wide modulation range of PA. Note that the magnitude of all the near- and far-field results are normalized to 1, for clearer comparison. We can observe that for the same incident energy, the metasurface element can achieve different amplifications. These different magnitudes can be clearly distinguished by the receiver, and here we encode them as "0," "1," "2," and "3" to represent the 2-bit digital information.

To clearly demonstrate the controllable amplification of the PA, we design and measure a transmission-line board embedded with an amplifier, as shown in Fig. 5(a). We provide different supply voltages and input powers, to test the amplification levels. The measured $S21$ results are presented in Fig. 5(b), in which the different input powers are marked in different colors. For example, when the input

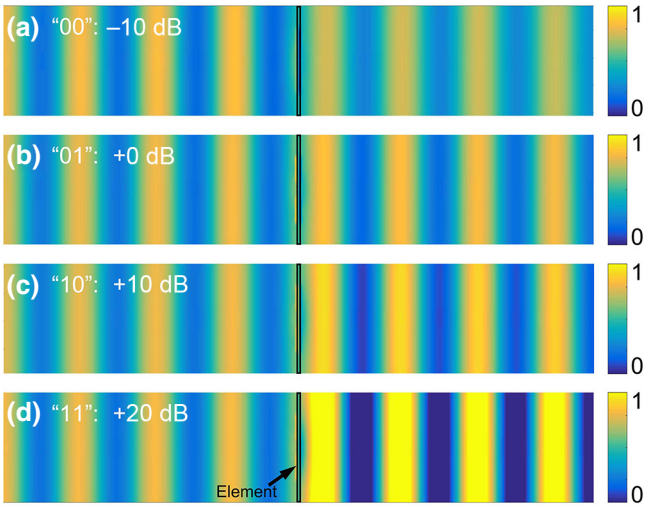

FIG. 4. The simulated near- and far-field results of the designed element, with different amplification levels. (a)–(d) The amplification levels are -10, 0, 10, and 20 dB, respectively, which are encoded as "00," "01," "10," and "11."

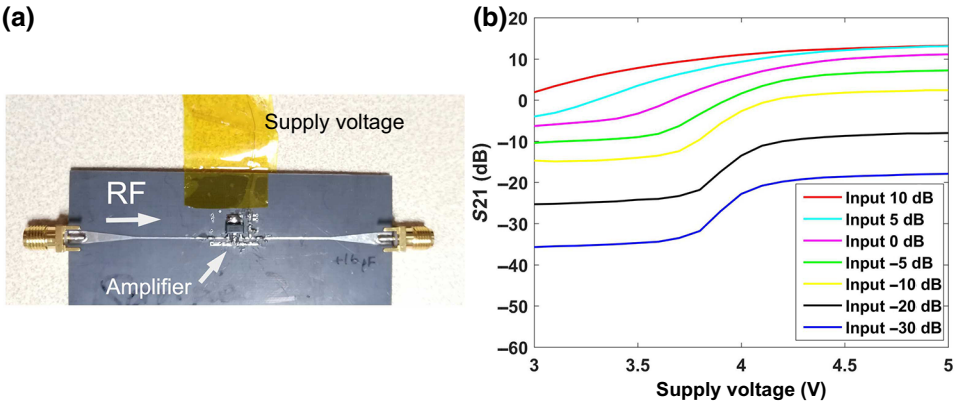

FIG. 5. The fabricated transmission-line board embedded with an amplifier and the measured gains with different supply voltages and input powers. (a) The fabricated transmission-line board embedded with an amplifier. (b) The measured $S21$ with different supply voltages.

is −30 dB, we can clearly observe that, with the increasing supply voltage, the amplification of the PA increases from about −7 to +13.5 dB. According to our measured results, when the input energy is less than or equal to −10 dB, an energy manipulation range of a single amplifier of about 20 dB can be achieved. As the input power is further increased, the amplification range will gradually decrease due to the power limitation of the amplifier itself. When the input power is 10 dB, the amplification range is decreased to about 10 dB. In this work, the amplifiers are used to magnify the energy of the space EM waves. We note that only one amplifier is measured on the microstrip board, so the largest amplification is about 13 dB. Moreover, we apply two amplifiers in each metasurface element, to realize a wider manipulation range. As a result, an amplification range from −10 to +20 dB in our design can be realized based on the above analysis.

In our experiment, we fabricate and measure a metasurface composed of 7×7 elements, integrating 98 amplifiers in total, as shown in Fig. 6(a). The designed sample has a dimension of 340×340 mm^2 and is fabricated with PCB technology, where copper is used as the metal. Amplifiers and other components are assembled by machine soldering. The measurements are performed in a standard anechoic chamber, to test the far-field results in a two-dimensional (2D) plane, as shown in Fig. 6(b). To show the connecting condition of the measurement clearly, a concise connection is provided in Fig. 6(c). Two broadband rectangular horns are employed as the transmitter and receiver, which are connected to the vector network analyzer to

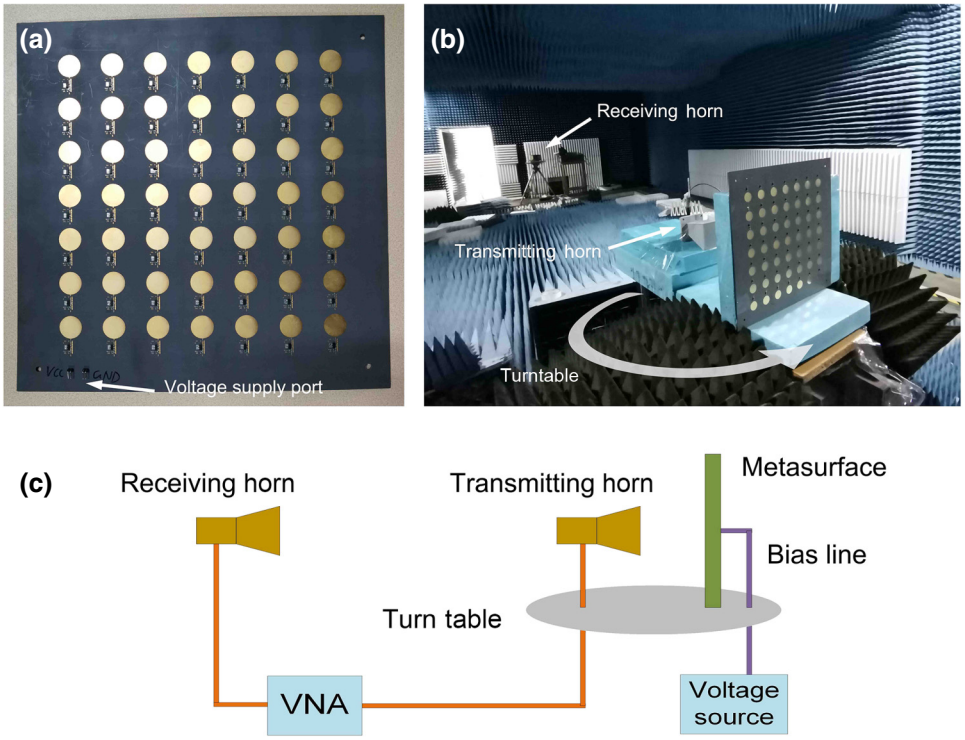

FIG. 6. The fabricated metasurface sample and measurement environment. (a) The fabricated 7×7 metasurface sample. (b) The photograph of the measurement environment. (c) The connecting condition in the measurement.

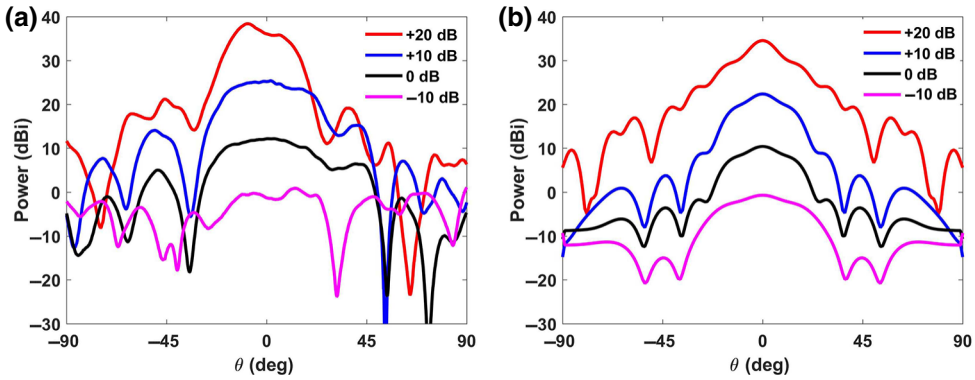

FIG. 7. Comparison of the simulated and measured far-field results of the designed metasurface with different amplification levels. (a) The simulated results. (b) The measured results.

measure the far-field results. The transmitter and metasurface samples are fixed on a turntable, in which a voltage source supplies PAs on the metasurface.

The measured results in the far-field region are illustrated in Fig. 7(b), and numerical simulations are also given in Fig. 7(a) for clear comparison. In the simulation for the whole metasurface, the same size rectangular horn is applied as that in the measurement. The operating frequency is set as 5 GHz. Four distinct amplification levels (20, 10, 0, and −10 dB) are provided to demonstrate the manipulation performance. The related four supply voltages are 3, 3.8, 4.2, and 5 V. The numerical results for the far-field region are also performed in CST MICROWAVE STUDIO, in which the plane-wave excitation is applied in full-wave simulations. The measured results have good agreement with the simulations, validating our design. The errors are mainly due to the following reasons: (1) the fabrication accuracy limitations of the PCB technology; (2) manual operations in the fabrications and measurements; and (3) the error in nonideal circuit components. The error in the power amplifier and its related components may contribute the most to this asymmetry. Since all power amplifiers are applied at the same voltage, the difference in the load resistance of the PA results in the difference in the amplifications. Hence, the far-field results show slight asymmetry comparing to the simulations.

IV. CONCLUSION

In summary, we propose a spatial-energy digital-coding metasurface to realize arbitrary manipulations in the energy of spatial propagating waves. We show that the amplification level of the PA can be determined by the supply voltage. Based on this property, the transmission energy can not only be reduced, but can also be increased as required. A 7×7 coding metasurface integrated with 98 amplifiers is designed, fabricated, and measured at 5 GHz. The measurement results have great consistency with our designs and simulations. Four different amplification levels from −10 to 20 dB are realized, implying the good performance of our design. We believe that this work may promote more integration between metasurfaces and traditional rf components, and also broaden the application potential for active and programmable metasurfaces.

ACKNOWLEDGMENTS

This work was supported in part by the National Key Research and Development Program of China (Grants No. 2017YFA0700201, No. 2017YFA0700202, and No. 2017YFA0700201), in part by the National Natural Science Foundation of China (Grants No. 61631007, No. 61571117, No. 61501112, No. 61501117, No. 61522106, No. 61731010, No. 61735010, No. 61722106, No. 61701107, No. 61701108, and No. 11404207), and in part by the 111 Project (Grant No. 111-2-05), SHIEP Foundation (Grants No. K2014-054 and No. Z2015-086), and the Local Colleges and Universities Capacity Building Program of the Shanghai Science and Technology Committee, China (Grant No. 15110500900).

[1] A. Arbabi, Y. Horie, M. Bagheri, and A. Faraon, Dielectric metasurfaces for complete control of phase and polarization with subwavelength spatial resolution and high transmission, Nat. Nanotechnol. **10**, 937 (2015).

[2] A. A. High, R. C. Devlin, A. Dibos, M. Polking, D. S. Wild, J. Perczel, N. P. de Leon, M. D. Lukin, and H. Park, Visible-frequency hyperbolic metasurface, Nature **522**, 192 (2015).

[3] A. Pors, M. G. Nielsen, R. L. Eriksen, and S. I. Bozhevolnyi, Broadband focusing flat mirrors based on plasmonic gradient metasurfaces, Nano Lett. **13**, 829 (2013).

[4] F. Aieta, P. Genevet, M. A. Kats, N. Yu, R. Blanchard, Z. Gaburro, and F. Capasso, Aberration-free ultrathin flat lenses and axicons at telecom wavelengths based on plasmonic metasurfaces, Nano Lett. **12**, 4932 (2012).

[5] Q. Wang, X. Zhang, Y. Xu, Z. Tian, J. Gu, W. Yue, S. Zhang, J. Han, and W. Zhang, A broadband metasurface-based terahertz flat-lens array, Adv. Opt. Mater. **3**, 779 (2015).

[6] Q. Ma, C. B. Shi, T. Y. Chen, M. Q. Qi, Y. B. Li, and T. J. Cui, Broadband metamaterial lens antennas with special properties by controlling both refractive-index distribution and feed directivity, J. Opt. **20**, 045101 (2018).

[7] C. Argyropoulos, K. Q. Le, N. Mattiucci, G. D'Aguanno, and A. Alu. Phys. Rev. B **87**, 205112 (2013).

[8] M. Khorasaninejad, W. T. Chen, R. C. Devlin, J. Oh, A. Y. Zhu, and F. Capasso, Metalenses at visible wavelengths: Diffraction-limited focusing and subwavelength resolution imaging, Science **352**, 1190 (2016).

[9] Q. Yang, J. Gu, D. Wang, X. Zhang, Z. Tian, C. Ouyang, R. Singh, J. Han, and W. Zhang, Efficient flat metasurface lens for terahertz imaging, Opt. Express **22**, 25931 (2014).

[10] X. Yin, Z. Ye, J. Rho, Y. Wang, and X. Zhang, Photonic spin Hall effect at metasurfaces, Science **339**, 1405 (2013).

[11] N. Yu, P. Genevet, M. A. Kats, F. Aieta, J. P. Tetienne, F. Capasso, and Z. Gaburro, Light propagation with phase discontinuities: Generalized laws of reflection and refraction, Science **334**, 333 (2011).

[12] T. J. Cui, M. Q. Qi, X. Wan, J. Zhao, and Q. Cheng, Coding metamaterials, digital metamaterials and programmable metamaterials, Light Sci. Appl. **3**, e218 (2014).

[13] S. Liu, T. J. Cui, L. Zhang, Q. Xu, Q. Wang, X. Wan, J. Q. Gu, W. X. Tang, M. Q. Qi, J. G. Han, W. L. Zhang, X. Y. Zhou, and Q. Cheng, Convolution operations on coding metasurface to reach flexible and continuous controls of terahertz beams, Adv. Sci. **3**, 1600156 (2016).

[14] T. J. Cui, S. Liu, and L. L. Li, Information entropy of coding metasurface, Light Sci. Appl. **5**, e16172 (2016).

[15] L. Zhang, X. Q. Chen, S. Liu, Q. Zhang, J. Zhao, J. Y. Dai, G. D. Bai, X. Wan, Q. Cheng, G. Castaldi, V. Galdi, and T. J. Cui, Space-time-coding digital metasurfaces, Nat. Commun. **9**, 4334 (2018).

[16] L. Li, T. J. Cui, W. Ji, S. Liu, J. Ding, X. Wan, L. Y. Bo, M. Jiang, C. W. Qiu, and S. Zhang, Electromagnetic reprogrammable coding-metasurface holograms, Nat. Commun. **8**, 197 (2017).

[17] L. H. Gao, Q. Cheng, J. Yang, S. J. Ma, J. Zhao, S. Liu, H. B. Chen, Q. He, W. X. Jiang, H. F. Ma, Q. Y. Wen, L. J. Liang, B. B. Jin, W. W. Liu, L. Zhou, J. Q. Yao, P. H. Wu, and T. J. Cui, Broadband diffusion of terahertz waves by multi-bit coding metasurfaces, Light Sci. Appl. **4**, e324 (2015).

[18] L. J. Liang, M. Q. Qi, J. Yang, X. P. Shen, J. Q. Zhai, W. Z. Xu, B. B. Xu, W. W. Liu, Y. J. Feng, C. H. Zhang, H. Lu, H. T. Chen, L. Kang, W. W. Xu, J. Chen, T. J. Cui, P. H. Wu, and S. G. Liu, Anomalous terahertz reflection and scattering by flexible and conformal coding metamaterials, Adv. Opt. Mater. **3**, 1374 (2015).

[19] Q. Ma, C. B. Shi, G. D. Bai, T. Y. Chen, A. Noor, and T. J. Cui, Beam-editing coding metasurfaces based on polarization bit and orbital-angular-momentum-mode bit, Adv. Opt. Mater. **5**, 1700548 (2017).

[20] L. Liu, X. Zhang, M. Kenney, X. Su, N. Xu, C. Ouyang, Y. Shi, J. Han, W. Zhang, and S. Zhang, Broadband metasurfaces with simultaneous control of phase and amplitude, Adv. Mater. **26**, 5031 (2014).

[21] Y. Xie, W. Wang, H. Chen, A. Konneker, B. I. Popa, and S. A. Cummer, Wavefront modulation and subwavelength diffractive acoustics with an acoustic metasurface, Nat. Commun. **5**, 5553 (2014).

[22] L. Huang, X. Chen, H. Mühlenbernd, H. Zhang, S. Chen, B. Bai, Q. Tan, G. Jin, K. W. Cheah, C. W. Qiu, J. Li, T. Zentgraf, and S. Zhang, Three-dimensional optical holography using a plasmonic metasurface, Nat. Commun. **4**, 2808 (2013).

[23] X. Ni, A. V. Kildishev, and V. M. Shalaev, Metasurface holograms for visible light, Nat. Commun. **4**, 2807 (2013).

[24] Y. W. Huang, H. W. Lee, R. Sokhoyan, R. A. Pala, K. Thyagarajan, S. Han, D. P. Tsai, and H. A. Atwater, Gate-tunable conducting oxide metasurfaces, Nano Lett. **16**, 5319 (2016).

[25] Y. Yao, R. Shankar, M. A. Kats, Y. Song, J. Kong, M. Loncar, and F. Capasso, Electrically tunable metasurface perfect absorbers for ultrathin mid-infrared optical modulators, Nano Lett. **14**, 6526 (2014).

[26] O. Buchnev, N. Podoliak, M. Kaczmarek, N. I. Zheludev, and V. A. Fedotov, Electrically controlled nanostructured metasurface loaded with liquid crystal: toward multifunctional photonic switch, Adv. Opt. Mater. **3**, 674 (2015).

[27] S. Taravati, B. A. Khan, S. Gupta, K. Achouri, and C. Caloz, Nonreciprocal nongyrotropic magnetless metasurface, IEEE Trans. Antenn. Propag. **65**, 3589 (2017).

[28] Z. Wang, Z. Wang, J. Wang, B. Zhang, J. Huangfu, J. D. Joannopoulos, M. Soljačić, and L. Ran, Gyrotropic response in the absence of a bias field, Proc. Natl. Acad. Sci. U.S.A. **109**, 13194 (2012).

[29] L. Xu, D. Chen, C. A. Curwen, M. Memarian, J. L. Reno, T. Itoh, and B. S. Williams, Metasurface quantum-cascade laser with electrically switchable polarization, Optica **4**, 4 (2017).

[30] M. Kim, J. J. Rosenberg, R. P. Smith, R. M. Weikle, J. B. Hacker, M. P. Delisio, and D. B. Rutledge, A grid amplifier, IEEE Microw. Wirel. Co. **1**, 322 (1991).